Half-metallicity in NiMnSb: A variational cluster approach with *ab initio* parameters

H. Allmaier,[1,][*] L. Chioncel,[1,2] E. Arrigoni,[1] M. I. Katsnelson,[3] and A. I. Lichtenstein[4]

[1]*Institute of Theoretical and Computational Physics, Graz University of Technology, A-8010 Graz, Austria*
[2]*Faculty of Science, University of Oradea, Oradea RO-47800, Romania*
[3]*Institute for Molecules and Materials, Radboud University of Nijmegen, NL-6525 ED Nijmegen, The Netherlands*
[4]*Institute of Theoretical Physics, University of Hamburg, 20355 Hamburg, Germany*
(Received 21 September 2009; revised manuscript received 17 December 2009; published 17 February 2010)

Electron correlation effects in the half-metallic ferromagnet NiMnSb are investigated within a combined density functional and many-body approach. Starting from a realistic multiorbital Hubbard model including Mn d and Ni d orbitals, the many-body problem is addressed via the variational cluster approach using, as a reference system, a two-site cluster containing one manganese and one nickel site. The density of states obtained in the calculation shows a strong spectral-weight transfer toward the Fermi level in the occupied conducting majority spin channel with respect to the uncorrelated case, as well as states with vanishing quasiparticle weight in the minority-spin gap. Although the two features produce competing effects, the overall outcome is a strong reduction in the spin polarization at the Fermi level with respect to the uncorrelated case. Our results indicate the presence of substantial nonlocal correlation effects in the low-energy range for minority-spin electrons. More specifically, the imaginary part of the self-energy between $Mn(t_{2g})$ and $Ni(t_{2g})$ orbitals is significantly larger than local contributions at those energies. This emphasizes the importance of nonlocal correlations in this material.

PACS number(s): 75.50.Cc, 71.10.Fd, 71.20.−b, 71.27.+a

I. INTRODUCTION

More than twenty years ago, de Groot *et al.*[1] carried out electronic structure calculations for the half-Heusler compound NiMnSb, which showed peculiar magnetic features leading to the discovery of a new class of materials, the so-called half-metallic ferromagnets. Such materials differ from conventional ferromagnets in that they display a gap in one of the spin channels only. The concept of half-metallicity boosted the research in spintronics—an emergent technology that makes use of spin and charge of electrons at the same time. Spintronic applications such as spin-valves, polarized electron injectors/detectors or devices using tunneling and giant magnetoresistance effects promise to revolutionize microelectronics once highly polarized electrons can be injected efficiently at room temperatures.[2,3]

Unfortunately, the theoretically predicted ideal full spin polarization of half-metals has not yet been found experimentally. As a matter of facts, experiments show that full polarization is lost at temperatures of the order of room temperature, and even at lower temperatures different factors such as structural inhomogeneities, as well as surfaces and interface properties may suppress it.[4,5]

Despite the fact that high quality NiMnSb films have been successfully grown, they were not found to reproduce the half-metallic character of the bulk suggested by spin-polarized positron-annihilation.[6,7] Values of spin polarization were reported between 40% in spin-resolved photoemission measurements[8] up to $58 \pm 2.3\%$ by superconducting point contact measurements[2] (see also Refs. 9 and 10). The discrepancy between theoretical calculations[1] and the above mentioned experimental facts were attributed to surface and interface effects. Consequently, different surface and interfaces of NiMnSb were theoretically investigated by de Wijs and de Groot,[4] which demonstrated that

half-metallicity can be preserved at the surface and/or interface by suitable reconstruction. The theoretical situation is complicated by the fact that the spin polarization (or, more precisely the tunneling magnetoresistance) displays a substantial uniaxial anisotropy in epitaxial grown NiMnSb, as was demonstrated previously.[11]

Recently, finite-temperature correlation effects were addressed in several half-metals.[5,12–16] For NiMnSb, a local density approximation plus dynamical mean field theory (LDA+DMFT) (Ref. 12) calculation showed the appearance of so-called nonquasiparticle (NQP) states. These states originate from spin-polaron processes, whereby the spin-down low-energy electron excitations, which are forbidden for half-metallic ferromagnets in the one-particle picture, turn out to be possible as superpositions of spin-up electron excitations and virtual magnons.[5,17–19] Here, we extend this study by adopting the variational cluster approach (VCA), which includes correlations beyond the locality captured by DMFT. In addition, the VCA is based on exact diagonalization, which is more appropriate than the diagrammatic spin polarized T-matrix fluctuation exchange (SPTF) method[20–22] adopted in Ref. 12 to solve the impurity problem. In a previous paper,[23] we used the VCA to investigate the spin polarization in NiMnSb taking into account only the Mn d orbital basis set. Our calculations showed that the Mn d-only basis set is not sufficient to appropriately describe the low-energy spectrum of NiMnSb around the Fermi level. For this reason, in the present work, we adopt a multiorbital Hubbard-type Hamiltonian written in a basis that includes all 10 orbitals of Mn d and Ni d states. Our present calculation confirms that the inclusion of the latter is essential for a proper description of ferromagnetic properties and of the minority-spin gap in NiMnSb.

Our results support the existence of states within the minority-spin gap in agreement with previous LDA +DMFT calculations.[5,12] In addition, they indicate that these

so-called nonquasiparticle states indeed have a vanishing quasiparticle weight at the Fermi energy. At the same time, our results predict a correlation-induced spectral-weight transfer for the majority spin states. The combination of these two effects yields a polarization whose energy dependence is in qualitative agreement with experiments. Our calculations emphasize the importance of nonlocal correlation effects. In particular, we show that the imaginary part of the self-energy for nearest-neighbor Ni and Mn sites is larger than the local one in the interesting region just above the Fermi energy for minority-spin states. The diagonal self-energy is in turn similar to the one obtained from the local DMFT construction discussed previously.[5,12] These calculations lead to the conclusion that even in the presence of medium-size interactions, nonlocal electron correlations significantly affect the spin polarization in half-metals.

This paper is organized as follows: in Sec. II, we present the methods used to investigate the electronic structure of NiMnSb. In particular, in Sec. II A, we describe the *ab initio* construction of the many-body model Hamiltonian. Specifically, the uncorrelated part of the Hamiltonian for excitations in the vicinity of the Fermi level is obtained from the so-called downfolding technique[24,25] within the Nth-order muffin tin orbital (NMTO) method. In Sec. II B, we give a short summary of the VCA approach. We present and discuss our results in Sec. III. In particular, in Sec. III A, we evaluate the density of states within VCA and discuss the results in the framework of previous calculations. In Sec. III B, we discuss *k*-dependent spectral properties, namely, the comparison between the spectral function and the band structure. Local and nonlocal self-energies are discussed in Sec. III C. Finally, spin polarization and its comparison with experiments is discussed in Sec. III D, and the summary of the results is presented in Sec. IV.

II. ELECTRONIC STRUCTURE CALCULATIONS FOR NiMnSb

The intermetallic compound NiMnSb crystallizes in the cubic structure of MgAgAs type (C1$_b$) with the fcc Bravais lattice (space group $F\bar{4}3m=T_d^2$). This structure can be described as three interpenetrating fcc lattices of Ni, Mn, and Sb with the lattice parameter $a=11.20a_0$ (a_0=Bohr radius), respectively. The Ni and Sb sublattices are shifted relative to the Mn sublattice by a quarter of the [111] diagonal in opposite directions, see also Fig. 1. The important aspects,[1,5,26–29] which determine the behavior of electrons near the Fermi level, as well as the half-metallic properties are the interplay between the crystal structure, the valence electron count, the covalent bonding, and the large exchange splitting of Mn *d* electrons. For the minority-spin gap opening, not only the Mn *d*-Sb *p* interactions, but also Mn *d*-Ni *d* interactions have to be taken into account. In addition, the loss of inversion symmetry produced by the C1$_b$ structure (the symmetry lowering from O_h in the L2$_1$ structure to T_d in the C1$_b$ structure) are important for these effects. The existence of *sp*-valent Sb is crucial to provide stability to this compound.

The crystal structure is shown in Fig. 1. The positions occupied by atoms are represented by spheres. For illustra-
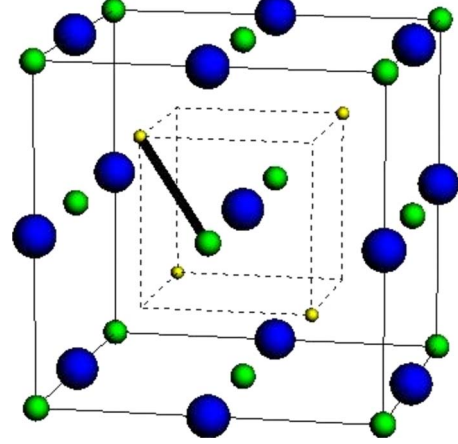

FIG. 1. (Color online) The conventional unit cell for the semi-Heusler NiMnSb compound: Sb (large, blue spheres) and Mn (medium, green spheres) sit on the same faces of the large cube (shown with thin, solid lines), Ni (small, yellow spheres) forms a separate (small) cube drawn using dashed lines. In addition, the atoms belonging to the reference system of the VCA calculation are connected by a thick solid line. Sb orbitals are downfolded and, therefore, not included directly in the model calculation.

tive purposes, in Fig. 1 the radii of the spheres were chosen arbitrarily. The actual muffin-tin radii used in the calculations are $R_{MT}^{Ni}=2.584$, $R_{MT}^{Mn}=2.840$, $R_{MT}^{Sb}=2.981$, and $R_{MT}^{E}=2.583$ (atomic units) for the vacant position situated in (1/4, 1/4, 1/4). The linear muffin-tin orbital basis within the atomic sphere approximation (LMTO-ASA) used for the self-consistent calculations contains the *spd*-partial waves for Mn and Ni, the *sp*(*df*)-partial waves for Sb and *s*(*pd*)-partial waves for the empty sphere *E*. (*l*) means that the *l*-partial waves are downfolded within the self-consistent calculations.

A. *Ab initio* construction of the model Hamiltonian

In order to construct the effective low-energy Hamiltonian to use in our VCA calculation, we employed the Nth-order muffin-tin-orbitals scheme within the LMTO-ASA basis set.[30] The NMTO method[24,25] can be used to generate truly minimal basis sets with a massive downfolding technique. Downfolding produces minimal bands which follow exactly the bands obtained with the full basis set. The minimal set of symmetrically orthonormalized NMTOs is a set of Wannier functions. In the construction of the NMTO basis set the active channels are forced to be localized onto the eigen-channel **R**lm, making the NMTO basis set strongly localized.

Fourier transformation of the orthonormalized NMTO Hamiltonian, $H^{LDA}(\mathbf{k})$, yields on-site energies and hopping integrals,

$$\langle \chi_{\mathbf{R}'m'}^{\perp,A}|H^{LDA}-\varepsilon_F|\chi_{\mathbf{R}m}^{\perp,B}\rangle \equiv t_{m',m}^{A-B,\mathbf{R}'-\mathbf{R}}, \quad (1)$$

in a Wannier representation, where the NMTO Wannier functions $|\chi_{\mathbf{R}m}^{\perp,A}\rangle$ are orthonormal. Here, $t_{m',m}^{A-B,\mathbf{R}'-R}$ denotes the hopping term from orbital m of atom B on-site $\mathbf{R}$ to the orbital m' of atom A on-site $\mathbf{R}'$ (A and B are either Ni or Mn)

Further information concerning technical details of the calculation can be found in Refs. 5 and 31.

In a previous paper,[31] we discussed the chemical bonding and computed model Hamiltonian parameters for the semi-Heusler NiMnSb using only Mn d Wannier orbitals. As mentioned above, not only the Mn d-Sb p, but also Mn d-Ni d interactions are required to open a gap in the minority spin channel: the minority occupied bonding states are mainly of Ni d character, while the unoccupied anti-bonding states are mainly of Mn d character. Therefore, in the present work we consider an enlarged NMTO basis consisting of Ni d and Mn d orbitals, which span an energy window of about ± 3 eV around the Fermi energy.

The matrix elements for the on-site energies $\epsilon_m^A \equiv t_{m,m}^{A-A,0}$ are given by (we use the convention in which $m = 1, \dots, 5$ corresponds to the d orbitals $\{xy, yz, zx, 3z^2 - 1, x^2 - y^2\}$ in the order)

$$\epsilon_m^{\text{Mn}} = (-1411, -1411, -1411, -721, -721), \quad (2)$$

$$\epsilon_m^{\text{Ni}} = (-2439, -2439, -2439, -2679, -2679). \quad (3)$$

The nearest-neighbor hopping terms are given by $[\mathbf{\Delta}_1 \equiv (-\frac{1}{4}, -\frac{1}{4}, -\frac{1}{4})]$

$$t_{m',m}^{\text{Ni-Mn},\mathbf{\Delta}_1} = \begin{pmatrix} -153 & -272 & -272 & -153 & 0 \\ -272 & -153 & -272 & 76 & -132 \\ -272 & -272 & -153 & 76 & 0 \\ 110 & -55 & -55 & 1 & 132 \\ 0 & 95 & -95 & 0 & 1 \end{pmatrix},$$

and the next-nearest-neighbor terms $[\mathbf{\Delta}_2 \equiv (\frac{1}{2}, -\frac{1}{2}, 0)]$

$$t_{m',m}^{\text{Mn-Mn},\mathbf{\Delta}_2} = \begin{pmatrix} -107 & -14 & 14 & 72 & 0 \\ 14 & 6 & 36 & -12 & 4 \\ -14 & 36 & 6 & 12 & 0 \\ 72 & 12 & -12 & 61 & 4 \\ 0 & -4 & -4 & 0 & -52 \end{pmatrix}, \quad (4)$$

$$t_{m',m}^{\text{Ni-Ni},\mathbf{\Delta}_2} = \begin{pmatrix} 142 & -53 & 53 & 129 & 0 \\ 53 & 229 & -71 & 133 & -92 \\ -53 & -71 & 229 & -133 & -92 \\ 129 & -133 & 133 & 40 & 0 \\ 0 & 92 & 92 & 0 & -51 \end{pmatrix}. \quad (5)$$

Here, all hoppings are given in units of meV, and only one representative hopping integral is shown for each class. Other hopping terms can be derived from proper unitary transformation using crystal symmetry (see, e.g., Ref. 32 for details). As one can see, the largest hoppings occur between the Wannier orbitals located on Ni and Mn atoms. In addition, there are further hopping terms in the Hamiltonian, which we do not show here for simplicity. We have taken into account hoppings up to a range of $r = 2.0a$. Neglected hoppings are about a factor 30 smaller than the largest nearest-neighbor hopping. The noninteracting part of the effective Hamiltonian for NiMnSb, thus, has the form

$$H_0 = \sum_{\mathbf{R}',\mathbf{R},\sigma} \sum_{\{A,B,m',m\}} t_{m',m}^{A-B,\mathbf{R}'-\mathbf{R}} c_{B\mathbf{R}'m'\sigma}^{\dagger} c_{A\mathbf{R}m\sigma}. \quad (6)$$

To take into account correlation effects, we add the spin-rotation invariant interaction H_I

$$H_I = \frac{1}{2} \sum_{\mathbf{R},A,\sigma,\sigma'} \sum_{m,n,o,p} U_{mnop} c_{A\mathbf{R}m\sigma}^{\dagger} c_{A\mathbf{R}n\sigma'}^{\dagger} c_{A\mathbf{R}p\sigma'} c_{A\mathbf{R}o\sigma}. \quad (7)$$

In Eqs. (6) and (7), $c_{A\mathbf{R}m\sigma}$ ($c_{A\mathbf{R}m\sigma}^{\dagger}$) are the usual fermionic annihilation (creation) operators acting on an electron with spin σ at site $\mathbf{R}$ in the orbital m of atom A. The Hamiltonian we are using includes spin- and pair-flip terms, as especially spin flip processes are important for a correct description of nonquasiparticle states.[5,14] For a realistic description of Coulomb interactions, the matrix elements U_{mnop} are computed for the particular material in terms of effective Slater integrals and Racah or Kanamori coefficients.[33,34] We use the same values of the effective Slater parameters for Mn and for Ni, i.e., $F^0 = 1.26$ eV, $F^2 = 5.58$ eV, and $F^4 = 3.49$ eV, which give a intraorbital Coulomb interaction of $U = U_{mmmm} = 2.0$ eV. Therefore, in our full-d model we unavoidably have orbital dependent Hund's rule couplings $J_{mm'mm'}$. In our work, the orbital-averaged value $\bar{J}$ of the $J_{mm'mm'}$, is equal to $\bar{J} = 0.65$ eV. For convenience, we parametrize the interactions of our model in terms of the physically more intuitive parameters U and $\bar{J}$, since the ratio $F^4/F^2 = 0.625$ (Refs. 35 and 36) can be considered to be fixed. In order to verify that our results do not depend significantly on the chosen U and $\bar{J}$-values, we carried out calculations for $U = 2.5$ eV and $U = 3$ eV and $\bar{J} = 0.78$ eV as well. This range of values corresponds to the one used in previous works.[12,13,37,38]

The on-site energies calculated in NMTO already contain effects from the Coulomb interaction at the LDA mean-field level. While this double counting can be absorbed into the chemical potential when only one set of degenerate orbitals is taken into account (see, e.g., Refs. 14 and 39), this is generally not possible if the full d orbitals and/or the orbitals of more than one inequivalent atom are used as basis set. Consequently, in order to avoid a double counting of the Coulomb contribution, the corresponding Hartree terms have to be subtracted from H_0.[40] This is achieved by replacing the onsite energies ϵ_m^A obtained from NMTO with[41]

$$\epsilon_m^{'A} = \epsilon_m^A$$
$$- \frac{1}{2} \left\{ U_{mmmm} \langle n_m^A \rangle - \sum_{m' \neq m} (2U_{mm'mm'} - U_{mm'm'm}) \langle n_{m'}^A \rangle \right\}. \quad (8)$$

$\langle n_m^A \rangle$ denotes the occupation of the *NMTO band* associated with atom A and orbital m. Notice that this is different from the occupation of the *orbital m* in atom A. The present double-counting procedure corresponds to the "around-mean-field" scheme.[40,42] In order to test the dependence on the double-counting schemes, we performed calculations considering different schemes, such as the "fully localized"

scheme and a combination of these two schemes as discussed in Ref. 40. From these tests, we find that our LDA+VCA results for the spectral function remain unchanged for energies within $E_F \pm 1$ eV, while for energies outside this range (from ± 1 eV to about ± 3 eV) a redistribution of Mn- and Ni-states is obtained.

B. Variational cluster approach

To solve the many-body Hamiltonian (6)+(7), we employ the variational cluster approach.[43,44] This method is an extension of cluster perturbation theory (CPT).[45–47] In CPT, the original lattice is divided into a set of disconnected clusters, and the intercluster hopping terms are treated perturbatively. VCA additionally includes "virtual" single-particle terms to the cluster Hamiltonian, yielding a so-called reference system, and then subtracts these terms perturbatively. The "optimal" value for these variational parameters is determined in the framework of the self-energy functional approach (SFA),[48,49] by requiring that the SFA grand-canonical potential Ω be stationary within this set of variational parameters. In this work, we only include the chemical potential of the cluster as a variational parameter, which is necessary in order to obtain a thermodynamically consistent particle density.[50,51] It is not necessary to include a ferromagnetic field in order to obtain a ferromagnetic phase, since the symmetry can be broken already at the finite-cluster level.[41] In this paper, we use a recently developed method, described in Ref. 52, to carry out the sum over Matsubara frequencies required in the evaluation of Ω, whereby an integral over a contour lying a finite (not small) distance from the real axis is carried out.

As a reference system, we use a cluster of two sites, representing one Mn atom and one Ni atom (see Fig. 1), each having the full-d manifold of five orbitals. Since we have to consider all five orbitals for each atom, it is very difficult to use larger clusters, which have to be exactly diagonalized many times in combination with the variational procedure.

III. RESULTS

A. Density of states

In order to study the influence of correlations on the half-metallic gap, we first display the spin-resolved local density of states in Fig. 2. Here, we present a comparison of the results obtained from local spin density approximation (LSDA) with the results from our LDA+VCA calculation. The LSDA-density of states (DOS) is mainly characterized by a large exchange splitting (about 3 eV) of the Mn d states, leading to large spin moments on the Mn site ($3.72\mu_B$). A small induced ferromagnetic moment is present on Ni ($0.29\mu_B$), while the Sb moment ($0.06\mu_B$) is antiparallel to the Mn moment. Overall, the calculated moments are in very good agreement with previous *ab initio* results.[1,5,27,29,31] The existence of large localized Mn moments of about $3.78\mu_B$ has been verified experimentally by neutron diffraction[53] as well as by the sum rule of the x-ray magnetic circular dichroism spectra.[54] These two experiments also confirm the magnitude of the LSDA-computed moments for Ni and Sb. The
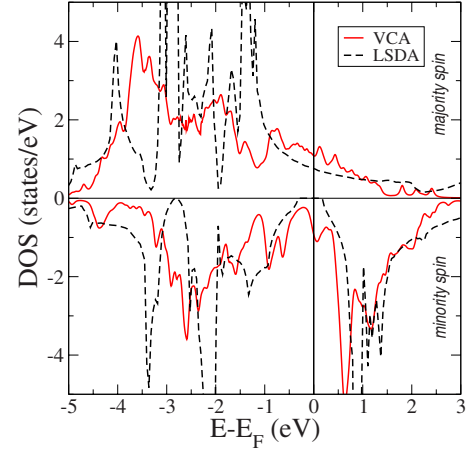

FIG. 2. (Color online) Density of states for NiMnSb obtained from LDA+VCA (red, solid line) for values of the average Coulomb and exchange parameters $U = 2$ eV and $\bar{J} = 0.65$ eV for both Mn and Ni atoms. In comparison to results obtained from LSDA (black, dashed line).

gap in the minority-spin channel is about 0.5 eV wide and the total magnetic moment has an integer value of $4\mu_B$. Note that in Fig. 2 in LSDA, the minority occupied bonding states are mainly of Ni d character, while unoccupied antibonding states are mainly of Mn d character. It was pointed out[1] that the opening of a gap is assisted by *Sb* through the symmetry lowering with the consequence that the distinction between Mn t_{2g} and Sb p character of the electrons is lost.

Concerning the LDA+VCA results, we find a total magnetic moment of $3.7\mu_B$, which is in reasonable agreement with experimental values.[53,54] In direct comparison to LSDA, our results show that correlation effects do not affect too strongly the general picture of the minority-spin DOS for energies, which are more than 0.5 eV away from the Fermi energy. In the range 0.5 eV $\lesssim E - E_F \lesssim 3$ eV, unoccupied Mn states are visible in the minority-spin sector, similarly to LSDA. However, these states are shifted to lower energies due to a slight reduction in the Mn-exchange splitting generated by the many-body correlations. Just above the Fermi level, NQP states are present, with a peak around the energy of 0.06 eV. It is important to note that these states were also obtained in previous calculations using a LDA+DMFT many-body approach[12] at finite temperatures. In comparison to the DMFT description, the nonlocal correlations captured by VCA enhance the spectral weight of the NQP states and slightly shift their position. We argue that this spectral-weight enhancement is caused by nonlocal contributions to the imaginary part of the self-energy which, as discussed in Sec. III C below, turn out to be larger than local contributions in the relevant energy range. As a matter of fact, the density of NQP states is proportional to the imaginary part of the self-energy, as discussed in Refs. 5, 17, and 19. Comparing our results with previous DMFT calculations,[12] one can conclude that, although the local DMFT description predicts a weaker spectral weight for NQP states, it is still sufficient to detect their existence. The spectral weight of NQP states is large enough, so that we expect them to be well pronounced in corresponding experimental data. While model calcula-

tions for single-band Hamiltonians[5] suggest that NQP states should only touch the Fermi level with zero weight at $T=0$ K, in our VCA calculation they maintain a finite weight at the Fermi level, thus leading to a reduction in spin polarization, even at $T=0$ K. In the LSDA results, the bonding states below the Fermi level have dominant Ni d character and are responsible for the gap formation. While these states form a single peak at -1.5 eV in LSDA, the LDA+VCA results show a splitting into two peaks centered around -1 eV. One of these peaks is pushed closer to the Fermi level, while the other one is shifted to higher energies. The latter correlation effect is also seen in previous LSDA+DMFT results.[12]

A significantly stronger effect caused by many-body correlations is visible in the majority-spin channel (see Fig. 2). Here, we discuss the behavior in the same energy range within ± 3 eV around the Fermi level, since this is the energy window spanned by our NMTO basis. The LSDA density of states in this energy range is determined mainly by the covalent Ni-Mn d hybridization, and by the large exchange splitting of Mn d electrons.[1,5,31] At the Fermi level and above a reduced density of states is present. The density of states obtained from the LDA+VCA calculation shows a very strong spectral redistribution for the majority spin electrons: the LSDA peak situated around -3 eV is lowered in energy while in the energy range between -2 eV and E_F, a spectral-weight transfer toward the Fermi level takes place. In particular, the large LSDA peak at -1.5 eV is shifted to about -1 eV, which results in a significant contribution to the states at the Fermi level. Just above the Fermi level, at energies where NQP states are formed in the minority-spin channel, a resonance peak is present in the density of states of the majority-spin electrons. A further maximum of the density of states is present at 0.5eV. The meaning of this maximum will become clear in the Sec. III B where the **k**-resolved spectral functions are discussed. In contrast to our VCA calculation, DMFT results[12] do not change significantly the picture for the majority-spin states. Although the LDA+DMFT density of states shows a similar reduction in spectral weight for the peak at -2 eV, its position remains unchanged. The differences between these two results might be explained by the fact that within DMFT Mn and Ni atoms are only coupled via the general many-body and charge-self consistency conditions, while correlations are treated independently on the two atoms. In contrast, the present VCA approach treats correlations exactly on the length scale of the cluster. These interatom correlations are possibly responsible for the splitting of the covalent Ni-Mn d electron hybridization in the majority spin states. Due to the breaking of this hybridization, the Mn d exchange splitting is decreased, which could explain the slight shifts of the minority unoccupied and occupied majority Mn d states.

B. Spectral properties

In order to gain insight into the nonlocal features of the density of states, we compute the **k**-resolved spectral function $A(\mathbf{k}, \omega)$. Majority- and minority-spin spectral functions are presented in Figs. 3 and 4, respectively, with **k** following
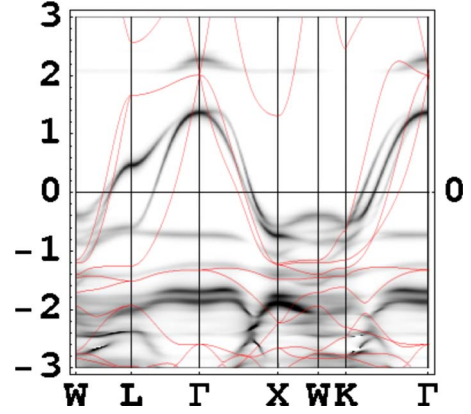

FIG. 3. (Color online) Majority spin LDA+VCA spectral function of NiMnSb (black/white density plot) along the conventional path in the BZ. $W(0.5,1,0)$ to $L(0.5,0.5,0.5)$ through $\Gamma(0,0,0)$, $X(0,1,0)$, and $K(0,0.75,0.75)$ points and ending at $\Gamma(0,0,0)$. The LSDA bands (red, thin solid lines) are shown for comparison. Parameters are as in Fig. 2.

high-symmetry points in the Brillouin zone (BZ). The explanation of the main features of the LSDA band structure was provided by de Groot *et al.* in his pioneering paper.[1] Emphasis was placed on the interaction between Mn and Sb connected by the symmetry constraint, while less attention was given to the Ni atom, although Mn and Ni are first neighbors and a strong hybridization between them is evidenced in the density of states. In our LDA+VCA calculation, Ni d and Mn d states are included explicitly, while Sb states are admixed by the downfolding procedure.

Due to correlation, the majority-spin bands crossing the Fermi energy are substantially narrowed with respect to the uncorrelated LSDA bands. Specifically, our results show for the bands crossing the Fermi level a reduction in the bandwidth from 3.2 to 2.2 eV. Along the path $W \rightarrow L$ both LSDA bands and the VCA spectral function cross the Fermi level at almost the same **k** point. The degenerate unoccupied level situated in the L-symmetry point, around 1.5 eV, is strongly pushed toward the Fermi energy, and determines the appear-
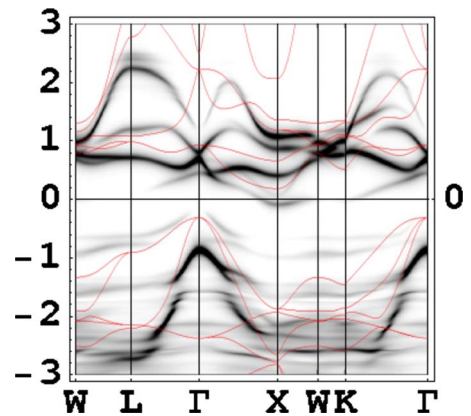

FIG. 4. (Color online) Minority-spin LDA+VCA spectral function of NiMnSb (black/white density plot) along the same BZ path as in Fig. 3. The LSDA bands (red, thin solid lines) are shown for comparison. Parameters are as in Fig. 2.

ance of the peak visible at 0.5 eV in the DOS discussed in Sec. III A. At the same time, correlation effects further split the degenerate levels at the Γ point seen in LSDA at around 2 eV. Note that along $\Gamma \rightarrow X$ crossing of the Fermi level occurs close to the corresponding crossings of the LSDA bands. Furthermore, along the path $X \rightarrow W \rightarrow K$ both VCA and LSDA bands are only weakly dispersive. However, the VCA bands are shifted toward the Fermi level, while along the line back into the Γ point, the Fermi energy crossing of the VCA bands takes place closer to the K point.

The minority-spin band structure of LSDA shows an indirect gap of about 0.5 eV between Γ and X point. Within this indirect gap formed by the mostly Ni d occupied and mostly Mn d unoccupied states, the LDA+VCA results show substantial spectral weight, as can be seen in Fig. 4. Notably, across the Fermi level a weakly dispersive band is present, centered around 0.1 eV, representing the NQP states. At higher energies, in the range of 1 to 2 eV above E_F, the VCA bands are substantially correlation-narrowed with respect to LSDA. The features above the Fermi level, including the nonquasiparticle states, have dominant Mn d character. Below the Fermi level, correlations split off the occupied bands having mainly Ni d character. The spectral weight is redistributed: a part is transferred toward the Fermi level, however with smaller weight, while most weight is transferred toward higher binding energies. The same effect is visible in the density of states plot displayed in Fig. 2. Notice that while the shift toward higher binding energies is also seen in the previous LSDA+DMFT calculation,[12] the weak shift toward the Fermi level is only obtained within the present calculation.

C. Local and nonlocal self-energies

In order to explore correlation effects in more detail, we plot in Fig. 5 the on-site total (i.e., traced over orbitals) self-energy on Mn and Ni sites on a large energy window $E = E_F \pm 5$ eV. The upper/lower panel of Fig. 5 shows the spin-resolved real/imaginary parts of the self-energy near the Fermi crossing at $k = (0.5, 0.7, 0.3)\pi/a$. Both Im Σ on Mn and Ni show a peak just above the Fermi level within the minority-spin channel, signaling the presence of NQP states in the density of states. The difference between majority and minority-spin contribution is significant in Mn owing to its large magnetic moment, while the small Ni moment agrees with the minor differences found between the self-energies of the minority and the majority spin channel.

Looking closer at the results for manganese, its minority-spin self-energy is significantly different in comparison to the self-energy of the majority spin channel. Especially just above the Fermi level, a clear peak in Im($\Sigma_{VCA}^{\downarrow}$) is present with a maximum around the energies of the nonquasiparticle states (Figs. 2 and 4). In previous DMFT calculations,[12] a very similar behavior of the imaginary part of the local self-energy was seen. In that case, the pronounced feature above E_F was attributed to the minority Mn $d(t_{2g})$ states. The real part of the self-energy displays a negative slope $\partial\Sigma/\partial\omega < 0$ at the Fermi energy for both spin directions, which confirms that the quasiparticle weight $Z = (1 - \frac{\partial\Sigma}{\partial\omega})^{-1}$ is reduced by cor-
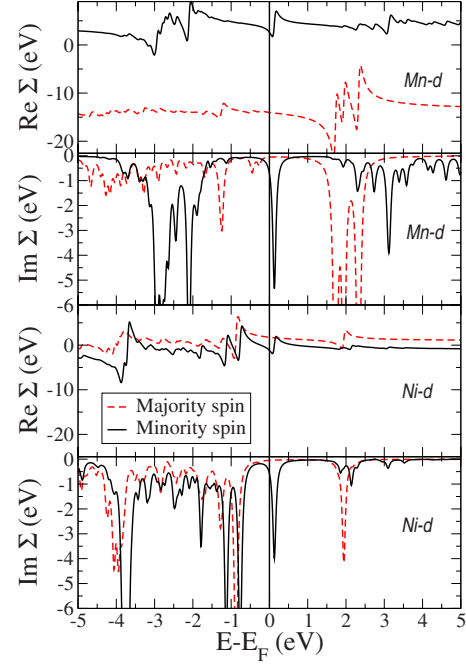

FIG. 5. (Color online) Spin resolved self-energies for Mn and Ni sites obtained as a sum of orbital-diagonal contribution, at the crossing point $k = (0.5, 0.7, 0.3)$. The strong Mn d spin splitting is due to the significant difference between majority and minority-spin self-energies, while the lack of magnetism on Ni is a consequence of similar spin-resolved self-energies.

relations. However, while for majority spins $|\partial\Sigma_{\uparrow}/\partial\omega|$ is clearly less than unity, for minority spins $|\partial\Sigma_{\downarrow}/\partial\omega| \gtrsim 1$ (within our approximation, we cannot determine Σ with sufficient accuracy), suggesting the nonquasiparticle nature of the minority-spin states within the gap.

To illustrate nonlocal correlation effects, we plot in Fig. 6 the majority-spin (upper panels) and the minority-spin (lower panels) imaginary parts of the local (left column) and nonlocal (right column) self-energies between various orbitals, on the energy scale of $E_F \pm 2$ eV around the Fermi level.

In the minority-spin channel, within this energy range, the largest term is the one connecting Mn(t_{2g}) and Ni(t_{2g}) orbitals just above the Fermi level. This is the energy at which NQP states appear in the density of states (Fig. 2). Notice that at the same energy, a strong local contribution to Im Σ is present as well. The additional nonlocal contribution results in an enhancement of the NQP-spectral weight as compared to its value obtained from DMFT calculations.[12] Notice that all other nonlocal contributions to Im Σ are significantly smaller.

In the local contributions below the Fermi energy, at about $E_F - 1$ eV two maxima are visible. In the minority-spin channel, the lower energy maximum is dominated by the Ni(t_{2g}) contribution, while the peak at higher energies is predominantly of Ni(e_g) character. These maxima contribute to the overall shift of Ni states toward the Fermi level, visible in the occupied part of the DOS in Fig. 2. These local orbital-diagonal contributions of Im(Σ) produce changes in the density of states that are similar to the ones obtained from the local DMFT-approach.[12]
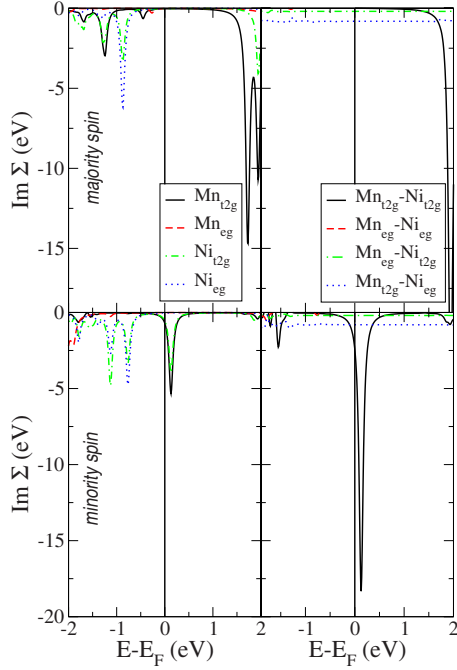
FIG. 6. (Color online) Imaginary part of the local and orbital-diagonal self-energy (left column). The right column shows the nearest-neighbor Im Σ.

For majority spin electrons, the site- and orbital diagonal contribution, shown in the upper left panel in Fig. 6, displays the same double peak structure at $E_F \approx -1$ eV for both $Ni(t_{2g})$ and $Ni(e_g)$ contributions as in the case of the minority-spin electrons. However, in contrast to the minority-spin contribution, the $Mn(t_{2g})$ contribution is visible and overlaps significantly with $Ni(t_{2g})$. At this energy, the $Ni(e_g)$ contribution is reduced, which causes an enhancement of the higher energy peak where $Ni(e_g)$ is dominant. There is no Mn contribution at all in the higher energy peak, however, at energies closer to E_F a second $Mn(t_{2g})$ peak is visible. This has important consequences for the majority spin density of states. The correlation-induced spectral-weight transfer toward the Fermi energy can be attributed to the appearance of self-energy contributions, which are site- and orbital-diagonal and close to the Fermi level. In addition, this contribution changes the $Mn(d)$-$Ni(d)$ hybridization. The majority spin site- and orbital-off-diagonal contributions, shown in the upper, right corner of Fig. 6, are less significant than its minority-spin analog.

The above analysis clearly emphasizes the influence of nonlocal correlations captured by the VCA, as well as the necessity to consider both Mn d and Ni d orbitals to obtain a complete picture for the low-energy physics in NiMnSb.

D. Low-energy spin polarization and comparison with experiments

To investigate the consequences of the modification of majority and minority spectral weight at the Fermi energy produced by correlations, we turn to the issue of the spin polarization. This is given by the expression $P(E) = [N_\uparrow(E) - N_\downarrow(E)]/[N_\uparrow(E) + N_\downarrow(E)]$, $N_\sigma(E)$ being the
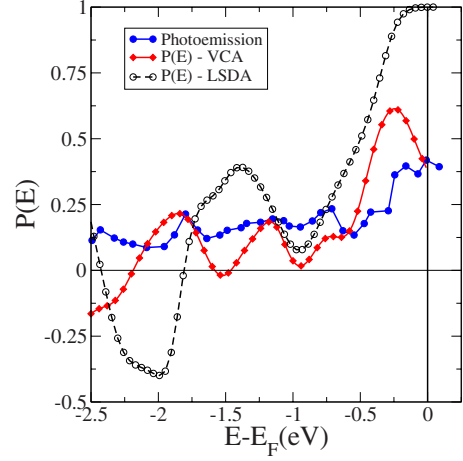

FIG. 7. (Color online) Energy-dependent polarization obtained from LSDA and LDA+VCA in comparison with data from spin-polarized photoemission (Ref. 8) (data used with kind permission from the authors).

spin-resolved density of states, and is plotted in Fig. 7 as a function of energy measured from the Fermi level. The computed LSDA and VCA values are compared with the raw data obtained from spin-resolved photoemission measurement by Zhu *et al.*[8] For this comparison, the density of states was multiplied with the Fermi function and a Gaussian broadening of 100 meV was used to account for experimental resolution. Zhu *et al.*[8] discuss the appearance of a shoulder close to the Fermi level when proper annealing is performed to restore the stoichiometry in NiMnSb. This shoulder is visible in the majority spin channel (Fig. 2c from Ref. 8) and could be an indication for the correlation-induced spectral-weight transfer of the majority spin states, not present in the LSDA calculations. In addition, the value of the spin polarization at the Fermi level obtained from our LDA+VCA results is situated in the interval of values reported experimentally.[2,8,55]

At the end of this section, we want to comment on the connection between the present approach and the seminal works of Edwards and Hertz,[17,56] followed by Irkhin and co-workers[18,19,57,58] to describe properties of itinerant electron ferromagnets using the Hubbard-model. In particular, the self-energy was computed for the interesting case of strong ferromagnetism, where all the electrons have only one spin direction (the half-metallic systems in discussion) using diagrammatic perturbation,[17,56] *s-d*, spin-wave theory,[19,57] or many-electron *X*-operator representation.[18,58] In a more physical picture, the self-energy represents the process of magnon emission and absorption by an electron as the electron's response to the fluctuating magnetic field that it sees as it moves through the crystal.[17,56] It was demonstrated that a such caused self-energy affects significantly the one-electron states by introducing nonquasiparticle contributions, which was later confirmed by numerical calculations in realistic materials.[5,12–16,38]

In the present paper, we have extended our previous LDA+DMFT results for NiMnSb (Refs. 5 and 12) in order to include many-body effects which are beyond the single-site description. A natural extension can be achieved using

the cluster perturbation theory, where interaction is treated exactly at the length scale of the cluster. As clusters including Mn-only basis sets are not sufficient to describe the low-energy features around Fermi energy,[59] we included here explicitly Ni d orbitals in the basis. Thus, the computed cluster contains two sites and a number of five orbitals are considered on each site. The magnon excitations arise owing to the spin dynamics, the spin- and pair-flip terms included in the Hamiltonian.

Note that, both in the framework of single-site DMFT and within this cluster method, the magnon dispersion cannot be properly taken into account when considering the effects of electron-magnon interaction since the magnon frequencies are replaced by some average value ω. This means that the detailed shape of the nonquasiparticle contributions to the density of states $(E-E_F \ll \hbar\omega)$, $\delta E \propto (E-E_F)^{3/2}$, see (Refs. [19], [56], and [58]), cannot be reproduced correctly in both these approaches. Notice, however, that the values of magnon frequencies are not essential to estimate the total spectral weight of the nonquasiparticle states and DOS in general at $E-E_F > \hbar\omega$, see also (Ref. [5]).

IV. SUMMARY

We have investigated the effects of correlations in NiMnSb using a combined LDA+VCA approach. The parameters for the effective noninteracting Hamiltonian were obtained using the downfolding procedure, for a basis including Ni d and Mn d orbitals. The multiorbital Hubbard-type many-body Hamiltonian was solved using the variational cluster approach for different values of $U_{\mathrm{Mn/Ni}}$ in the range of 2 and 3eV and for $J_{mm'mm'}$ for which the orbitally averaged value $\bar{J}_{\mathrm{Mn/Ni}}$ ranges between 0.65 and 0.78 eV. The results presented do not show significant differences for the studied range of parameters, nor for different double-counting procedures used. We showed that the presence of Ni d orbitals in the NMTO basis allows for a more complete description of the low-energy behavior of NiMnSb. In particular, it correctly describes the spectral-weight transfer toward the Fermi level in the majority spin channel and the formation of minority-spin states with vanishing quasiparticle weight (NQP states) just above the Fermi level. The analysis of the minority-spin spectral function shows for the NQP states a weakly dispersive band having dominantly Mn d character. Due to electron correlations, the covalent Ni-Mn-d hybridization in the majority-spin channel splits up and part of the weight is transferred toward the Fermi level. The *simultaneous* presence of majority spin spectral-weight transfer toward the Fermi level, and the occurrence of minority-spin nonquasiparticle states emphasizes the importance of correlation effects in this material, despite the small value of U. One should remark that our results were obtained in the ideal isotropic case, while it is known that epitaxially grown NiMnSb displays significant uniaxial anisotropy.[11] When taking into account this effect, we expect nonquasiparticle states to be shifted to higher energies away from the Fermi surface, due to the corresponding gap occurring in the magnon spectrum.

Despite the fact that high-quality films of NiMnSb have been grown, they do not reproduce the half-metallic character of the bulk detected by spin-polarized positron-annihilation.[6,7] On the other hand, one should mention that the positron-annihilation technique only provides an evidence for half-metallicity by means of a consistency check. In other words, the "proof" is carried out by modeling the data assuming a half-metallic band structure, with a full minority-spin gap, *from the outset*.[6,7] For this reason, it would be interesting to revisit the analysis of the positron-annihilation data by using the correlated band structure obtained here, i.e., by taking into account the existence of NQP states.

---

*hannes.allmaier@itp.tugraz.at

[1] R. A. de Groot, F. M. Mueller, P. G. van Engen, and K. H. J. Buschow, Phys. Rev. Lett. **50**, 2024 (1983).

[2] R. J. Soulen *et al.*, Science **282**, 85 (1998).

[3] I. Zutic, J. Fabian, and S. D. Sarma, Rev. Mod. Phys. **76**, 323 (2004).

[4] G. A. de Wijs and R. A. de Groot, Phys. Rev. B **64**, 020402 (2001).

[5] M. I. Katsnelson, V. Yu. Irkhin, L. Chioncel, A. I. Lichtenstein, and R. A. de Groot, Rev. Mod. Phys. **80**, 315 (2008).

[6] K. E. H. M. Hanssen and P. E. Mijnarends, Phys. Rev. B **34**, 5009 (1986).

[7] K. E. H. M. Hanssen, P. E. Mijnarends, L. P. L. M. Rabou, and K. H. J. Buschow, Phys. Rev. B **42**, 1533 (1990).

[8] W. Zhu, B. Sinkovic, E. Vescovo, C. Tanaka, and J. S. Moodera, Phys. Rev. B **64**, 060403 (2001).

[9] J. S. Correa, Ch. Eibl, G. Rangelov, J. Braun, and M. Donath, Phys. Rev. B **73**, 125316 (2006).

[10] J. Minar, J. Braun, S. Bornemann, and M. Donath, J. Phys. D **42**, 084009 (2009).

[11] J. Liu, E. Girgis, P. Bach, C. Rüster, C. Gould, G. Schmidt, and L. W. Molenkamp, J. Appl. Phys. **99**, 036110 (2006).

[12] L. Chioncel, M. I. Katsnelson, R. A. de Groot, and A. I. Lichtenstein, Phys. Rev. B **68**, 144425 (2003).

[13] L. Chioncel, Ph. Mavropoulos, M. Ležaić, S. Blügel, E. Arrigoni, M. I. Katsnelson, and A. I. Lichtenstein, Phys. Rev. Lett. **96**, 197203 (2006).

[14] L. Chioncel, H. Allmaier, E. Arrigoni, A. Yamasaki, M. Daghofer, M. I. Katsnelson, and A. I. Lichtenstein, Phys. Rev. B **75**, 140406 (2007).

[15] L. Chioncel, Y. Sakuraba, E. Arrigoni, M. I. Katsnelson, M. Oogane, Y. Ando, T. Miyazaki, E. Burzo, and A. I. Lichtenstein, Phys. Rev. Lett. **100**, 086402 (2008).

[16] L. Chioncel, E. Arrigoni, M. I. Katsnelson, and A. I. Lichtenstein, Phys. Rev. B **79**, 125123 (2009).

[17] D. M. Edwards and J. A. Hertz, J. Phys. F: Met. Phys. **3**, 2191 (1973).

[18] V. Y. Irkhin and M. I. Katsnelson, Sov. Phys. Solid State **25**, 1947 (1983).

[19] V. Y. Irkhin and M. I. Katsnelson, J. Phys.: Condens. Matter **2**, 7151 (1990).

[20] A. I. Lichtenstein and M. I. Katsnelson, Phys. Rev. B **57**, 6884 (1998).

[21] M. I. Katsnelson and A. I. Lichtenstein, J. Phys.: Condens. Matter **11**, 1037 (1999).

[22] M. I. Katsnelson and A. I. Lichtenstein, Eur. Phys. J. B **30**, 9 (2002).

[23] H. Allmaier *et al.*, J. Optoelectron. Adv. Mater. **10**, 1671 (2008).

[24] O. K. Andersen and T. Saha-Dasgupta, Phys. Rev. B **62**, R16219 (2000).

[25] E. Zurek, O. Jepsen, and O. K. Andersen, ChemPhysChem **6**, 1934 (2005).

[26] S. Öğüt and K. M. Rabe, Phys. Rev. B **51**, 10443 (1995).

[27] I. Galanakis, P. H. Dederichs, and N. Papanikolaou, Phys. Rev. B **66**, 134428 (2002).

[28] B. R. K. Nanda and I. Dasgupta, J. Phys.: Condens. Matter **15**, 7307 (2003).

[29] E. Kulatov and I. I. Mazin, J. Phys.: Condens. Matter **2**, 343 (1990).

[30] O. K. Andersen and O. Jepsen, Phys. Rev. Lett. **53**, 2571 (1984).

[31] A. Yamasaki, L. Chioncel, A. I. Lichtenstein, and O. K. Andersen, Phys. Rev. B **74**, 024419 (2006).

[32] E. Pavarini, A. Yamasaki, J. Nuss, and O. K. Andersen, New J. Phys. **7**, 188 (2005).

[33] M. Imada, A. Fujimori, and Y. Tokura, Rev. Mod. Phys. **70**, 1039 (1998).

[34] G. Kotliar, S. Y. Savrasov, K. Haule, V. S. Oudovenko, O. Parcollet, and C. A. Marianetti, Rev. Mod. Phys. **78**, 865 (2006).

[35] F. M. F. de Groot, J. C. Fuggle, B. T. Thole, and G. A. Sawatzky, Phys. Rev. B **42**, 5459 (1990).

[36] V. I. Anisimov, I. V. Solovyev, M. A. Korotin, M. T. Czyżyk, and G. A. Sawatzky, Phys. Rev. B **48**, 16929 (1993).

[37] L. Chioncel, M. I. Katsnelson, G. A. de Wijs, R. A. de Groot, and A. I. Lichtenstein, Phys. Rev. B **71**, 085111 (2005).

[38] L. Chioncel, E. Arrigoni, M. I. Katsnelson, and A. I. Lichtenstein, Phys. Rev. Lett. **96**, 137203 (2006).

[39] H. Allmaier, L. Chioncel, and E. Arrigoni, Phys. Rev. B **79**, 235126 (2009).

[40] A. G. Petukhov, I. I. Mazin, L. Chioncel, and A. I. Lichtenstein, Phys. Rev. B **67**, 153106 (2003).

[41] Notice that the initial NMTO calculation is carried out in the nonmagnetic phase, so that the starting Hamiltonian (6) plus Eq. (7) is spin independent. The ferromagnetic solution is then obtained variationally within the VCA approach. This is important in order to preserve a spin-rotation symmetric model Hamiltonian.

[42] M. T. Czyzyk and G. A. Sawatzky, Phys. Rev. B **49**, 14211 (1994).

[43] M. Potthoff, M. Aichhorn, and C. Dahnken, Phys. Rev. Lett. **91**, 206402 (2003).

[44] C. Dahnken, M. Aichhorn, W. Hanke, E. Arrigoni, and M. Potthoff, Phys. Rev. B **70**, 245110 (2004).

[45] C. Gros and R. Valenti, Phys. Rev. B **48**, 418 (1993).

[46] D. Sénéchal, D. Perez, and M. Pioro-Ladriere, Phys. Rev. Lett. **84**, 522 (2000).

[47] S. G. Ovchinnikov and I. S. Sandalov, Physica C **161**, 607 (1989).

[48] M. Potthoff, Eur. Phys. J. B **32**, 429 (2003).

[49] M. Potthoff, Eur. Phys. J. B **36**, 335 (2003).

[50] M. Aichhorn and E. Arrigoni, EPL **72**, 117 (2005).

[51] M. Aichhorn, E. Arrigoni, M. Potthoff, and W. Hanke, Phys. Rev. B **74**, 024508 (2006).

[52] X. Lu and E. Arrigoni, Phys. Rev. B **79**, 245109 (2009).

[53] C. Hordequin, J. Pierre, and R. Currat, Physica B **234-236**, 605 (1997).

[54] A. Kimura, S. Suga, T. Shishidou, S. Imada, T. Muro, S. Y. Park, T. Miyahara, T. Kaneko, and T. Kanomata, Phys. Rev. B **56**, 6021 (1997).

[55] S. K. Clowes, Y. Miyoshi, Y. Bugoslavsky, W. R. Branford, C. Grigorescu, S. A. Manea, O. Monnereau, and L. F. Cohen, Phys. Rev. B **69**, 214425 (2004).

[56] D. M. Edwards, J. Phys. C **16**, L327 (1983).

[57] M. I. Auslender and V. Y. Irkhin, Z. Phys. B **56**, 301 (1984).

[58] V. Y. Irkhin and M. I. Katsnelson, Phys. Rev. B **73**, 104429 (2006).

[59] H. Allmaier *et al.*, J. Optoelectron. Adv. Mater. **10**, 737 (2008).